RESEARCH ARTICLE

CrossMark

Eco-friendly and facile electrochemical synthesis of sub-micrometer lead powders in deep eutectic solvents using galena as a raw material

Juanjian Ru[1] · Jiaojiao Bu[1] · Zhiwei Wang[1] · Yixin Hua[1,2] · Ding Wang[1]

Abstract

The sub-micrometer lead powders were electrodeposited on a mild steel (MS) substrate in PbS-containing (10–50 mM) choline chloride–urea deep eutectic solvent (ChCl–urea DES) at 353 K and 2.5 V. The electrochemical behaviors of the Pb(II)/Pb on MS and glass carbon electrodes were determined by cyclic voltammetry and chronoamperometry measurement. It indicates that the reduction of Pb(II) is a quasi-reversible process. The increase in PbS concentration effectively promotes the $E_{Pb(II)/Pb}$ shift in positive direction which can facilitate the reduction of Pb(II). The initial nucleation stage of metallic lead on MS electrode is a three-dimensional instantaneous nucleation for diffusion control and the diffusion coefficient of Pb(II) at 353 K is about 2.40×10^{-7} cm^2/s. The three-dimensional sub-micrometer lead particles are agglomerated together and composed of many overlapped lead flakes about 150–200 nm. Moreover, the XRD results reveal that metallic lead can be deposited with a face-centered-cubic structure and the strongest peak intensity is (111) plane. This finding provides a theoretical guidance for the one-step preparation of sub-micrometer lead powders using galena concentrate as raw material by an eco-friendly and facile electrochemical approach in close neutral electrolyte, which can efficiently shorten the production flow and realize the integration of metallurgy and material processes.

Graphical abstract
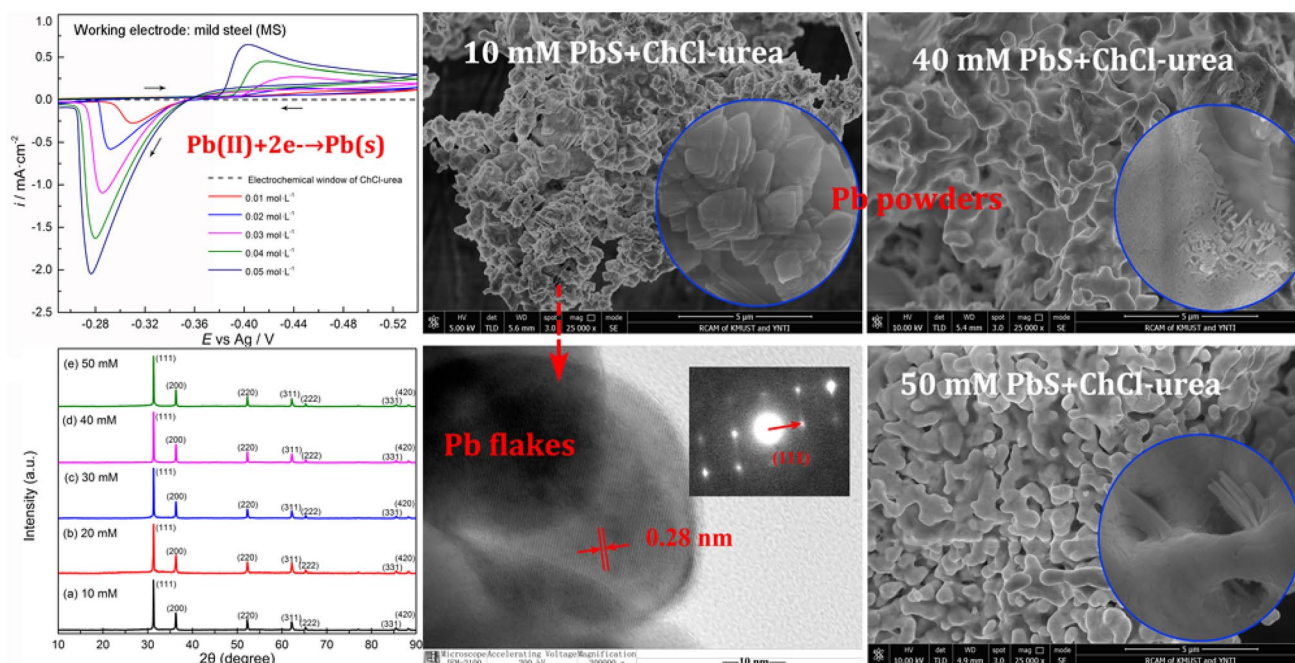
Extended author information available on the last page of the article

1 Introduction

Lead powders play very important roles as an active material in lead-acid battery, semiconductors, electrochromic devices, industry X-ray shield, radiological medical protective clothing and so on [1–3]. These applications require the manufacture of lead powders with high purity and quality. Several methods, such as mechanical ball milling and liquid metal atomization techniques, have been developed for the preparation of lead powders [4, 5]. Although these methods are supposed successful from a business perspective, the long production process and/or high requirements for equipment are the bottlenecks for the large-scale applications. Another method to obtain metal powders that has been used extensively is electrodeposition technique [6]. Nikolic et al. [7, 8] reported that the electrochemical and crystallographic aspects of lead formation in granular form were examined and compared in $NaNO_3$–$Pb(NO_3)_2$ solution. Han et al. [9] have fabricated a porous lead foam electrochemically at copper substrate with improved electrocatalytic performance for the electroreduction of CO_2 to formic acid. Porous lead films with high surface area can be electrodeposited using a hydrogen bubble dynamic template in $HClO_4$ containing $Pb(ClO_4)_2 \cdot 3H_2O$ [10]. In addition, the magnetic signature of electrodeposited lead nanowires from $Pb(H_2NSO_3)_2$ is also characterized [3]. According to above-mentioned literatures, the major merits of the electrodeposition technique are low equipment requirements, easy operation, controllable morphology, and high purity of metal powders [11, 12].

It is worth noting that currently used raw materials in lead electrodeposition process are finished chemical products, for instance, $Pb(ClO_4)_2$, $Pb(NO_3)_2$, $PbCl_2$. Therefore, the preparation process is complicated and the cost is unsatisfactory. The one-step preparation of lead powders from galena concentrate is optimum by electrodeposition technique in close neutral electrolyte. This can not only efficiently shorten the production flow but also realize the integration of metallurgy and material processes. Particularly, lead sulfide (PbS), the major components of galena, is the main raw materials for the recovery of metallic lead and widely distributed throughout nature associated with sphalerite, argentite pyrite, and so on. Thus, PbS can be seen as an appropriate candidate of the raw materials for producing lead powders. In addition, the primarily ionic systems called deep eutectic solvents (DESs) have been developed as promising electrolytes for large-scale electrolysis applications due to their chemical inertness with water, cheap and convenience [13–16]. In recent studies, several metals are obtained directly from their oxides, such as PbO [17–19], ZnO [20], CuO [21], SnO [22], thanks to the obvious differences in solubility for many oxides in DESs. However, to our knowledge for preparation of lead powders using PbS as raw material, no research have ever been conducted through an electrochemical approach in DESs.

Herein, the electrodeposition of coral-like lead sub-micrometer particles was investigated in PbS-containing (10–50 mM) ChCl–urea DES for the first time. Cyclic voltammetry and chronoamperometry measurement are carried out to study the electrochemical mechanism of lead deposition at different PbS concentrations. From a fundamental point of view, the effects of PbS concentrations on the morphologies and phase composition of products are elucidated by scanning electron microscopy (SEM), transmission electron microscope (TEM), and X-ray diffraction (XRD). This study provides a theoretical guidance for the one-step preparation of sub-micrometer lead powders using galena concentrate as raw material, which can efficiently shorten the production flow and realize the integration of metallurgy and material processes.

2 Experimental

The chemicals used in present study were purchased commercially with analytical grade from Aisinaladdin-e.com, Shanghai, China. As shown in Fig. 1, the PbS raw material is irregularly granular in particle size of 5–30 μm, and XRF testing shows that the purity of PbS is about 99.90%. Before use, PbS powders were dried under vacuum for 12 h at 353 K. The choline chloride and urea (mole ratio 1:2) were mixed at 353 K to prepare a homogeneous and colorless ChCl–urea DES. Then PbS powders with different amounts (10–50 mM) were added into the DES at 353 K for 12 h to form a PbS–ChCl–urea solution.

The electrochemical behavior measurements were conducted on an electrochemical workstation (Shanghai CH CHI760C model) at 10 mV s^{-1} and 353 K. A conventional three-electrode cell was employed in present experiments. The working electrodes were mild steel (MS) electrode and glass carbon (GC) electrode (0.1256 cm^2). An Ag/AgCl wire placed in a glass tube containing ChCl–urea was regard as quasi-reference electrode. A platinum wire was served as counter electrode. All electrodes were polished with metallographic abrasive paper, degreased with anhydrous ethanol in an ultrasonic bath, then washed with distilled water and dried.

Small-scale constant potential electrolysis experiment was carried out in a 50 cm^3 glass cell by direct current regulated power supply (DSP-305BF model). A MS substrate and a graphite sheet (3 cm^2) were served as the cathode and
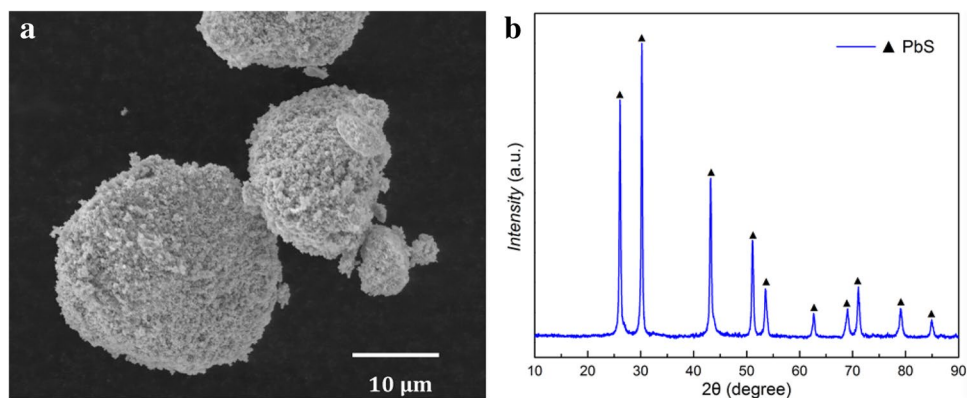
anode. Lead powders were electrodeposited on the MS substrate with an effective area of 3 cm^2. And the interelectrode distance between electrodes was 1.0 cm. All the electrodeposition experiments were controlled for 2 h in 10–50 mM PbS–ChCl–urea solution at 353 K and 2.5 V. Finally, the lead powders were took out from the glass cell and washed with anhydrous ethanol to removal adhered electrolyte and finally dried under vacuum.

The crystal structure of the lead powders stripped from MS substrate was analyzed with XRD (D/Max-2200 model) with a monochromatic Cu-Kα radiation at a scan rate of 10° min^{-1} in the range of $2\theta = 10°$–90°. The purity of samples was characterized by XRF (Epsilon3XLE model). The morphology and particle size of the lead powders were examined with SEM (XL 30 ESEM TMP model) and TEM (JEM-2100 model).

3 Results and discussion

3.1 Cyclic voltammetry

Figure 2a, c shows the cyclic voltammograms of a solution of 10–50 mM PbS in ChCl–urea DES at 353 K. The effects of PbS concentration (C_{PbS}) on the cathodic peak potential (E_{pc}) and peak current density (i_{pc}), obtained from Fig. 2, have been listed in Table 1. For clarity, the cyclic voltammogram of the MS electrode in 10 mM PbS–ChCl–urea DES is illustrated separately in Fig. 2b. The voltammogram is initiated from +0.25 V in negative direction and reversed at −0.54 V in positive direction. When the potential reaches point B (−0.36 V), the current value starts to increase which ascribed the onset of lead reduction in PbS–ChCl–urea DES. Then the current value increases gradually and reverses at point C (−0.54 V) with a continuous decline in positive direction. Therefore, a well-defined reduction peak occurs on MS electrode, while no reduction peak is observed at the same position in blank solution (dash line), suggesting that the peak is related to the reduction of Pb(II). Subsequently,

the current value reaches 0 at the crossover potential and a nucleation loop is formed between point B and point D (−0.42 V). This phenomenon can be ascribed to the overpotential needed to arouse the initial deposition stage of lead powders on a heterophase substrate, i.e., MS electrode and GC electrode [23]. The current then reaches anodic potential related to the stripping of the deposited lead. Therefore, the cathodic reaction can be represented as follow:

$$Pb(II) + 2e^- \rightarrow Pb \tag{1}$$

As shown in Fig. 2a, when the PbS concentration increases from 10 to 50 mM, the reduction potential of Pb(II)/Pb ($E_{Pb(II)/Pb}$) on MS electrode shifts obviously to more positive direction, about from −0.408 to −0.36 V. Apparently, there is a promotion effect on the reduction process of Pb(II) on MS electrode because of the positive shifting of the $E_{Pb(II)/Pb}$ and E_{pc}. As the PbS concentration increasing, the anodic peak potential (E_{pa}) shifts slightly to positive direction and the corresponding peak current density (i_{pa}) increases markedly. Moreover, the electrochemistry behavior of Pb(II) on GC electrode is similar to that on MS electrode, as shown in Fig. 2c. The nucleation loops are also detected. However, the $E_{Pb(II)/Pb}$ on GC electrode (about −0.477 V, 10 mM PbS) is more negative than that on MS electrode (Table 1). Meanwhile, with the increasing of PbS concentration, the $E_{Pb(II)/Pb}$ on GC electrode shifts significantly to more positive direction, about from −0.477 to −0.375 V. This variation tendency implies that the PbS concentration has a more obvious effect on the cyclic voltammograms of GC electrode compared with that of MS electrode mentioned above. By comparison, the electrochemical reduction of Pb(II) on GC electrode is more difficult than that on MS electrode, which can be ascribed to the substantial overpotential required to initiate the deposition process of lead on inert electrode. Thus, the electrodeposition of lead powders on active electrode, like MS electrode, will benefit to the nucleation of lead grains. The difference of the peak potentials ΔE_p ($= |E_{pa} - E_{pc}|$) are in the range of 127–167 mV and 220–534 mV on MS

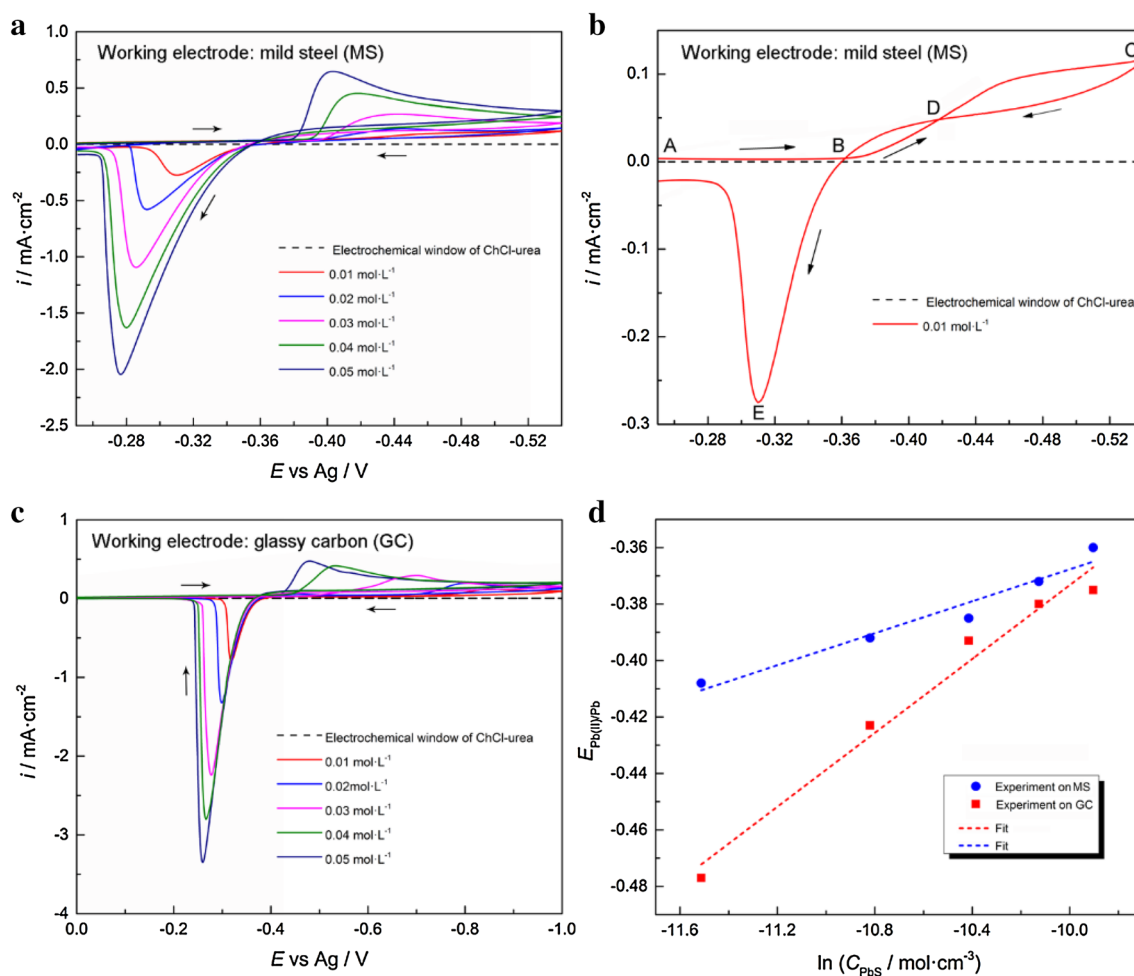**Fig. 2** Cyclic voltammograms of electrode at 353 K, sweep rate: 10 mV s^{-1}: **a** MS electrode, $C_{PbS} = 10$–50 mM; **b** MS electrode, $C_{PbS} = 10$ mM; **c** GC electrode, $C_{PbS} = 10$–50 mM; **d** plot of the deposition potential $E_{Pb(II)/Pb}$ against the logarithm of PbS concentration ln C_{PbS}

Table 1 Effect of C_{PbS} on the cyclic voltammograms on mild steel (MS) electrode and glassy carbon (GC) electrode in PbS–ChCl–urea solution

C_{PbS} (mM)	$E_{Pb(II)/Pb}$ (V)		E_{pc} (V)		E_{pa} (V)		ΔE_p (mV)		i_{pc} (mA cm^{-2})		i_{pa} (mA cm^{-2})	
	MS	GC	MS	GC	MS	GC	MS	GC	MS	GC	MS	GC
10	−0.408	−0.477	−0.477	−0.853	−0.310	−0.319	167	534	0.100	0.112	−0.275	−0.796
20	−0.392	−0.423	−0.451	−0.803	−0.293	−0.299	158	504	0.154	0.191	−0.572	−1.326
30	−0.385	−0.393	−0.441	−0.700	−0.286	−0.275	155	425	0.268	0.289	−1.094	−2.213
40	−0.372	−0.380	−0.418	−0.529	−0.280	−0.264	138	265	0.454	0.407	−1.628	−2.782
50	−0.360	−0.375	−0.403	−0.479	−0.276	−0.259	127	220	0.648	0.471	−2.042	−3.352

and GC electrode. Both values are much larger than the theoretical values of 2.3RT/nF (35 mV at 353 K) in reversible process (Table 1) [24]. Therefore, the electroreduction of Pb(II) in 10–50 mM PbS–ChCl–urea solution is a quasi-reversible process.

Based on above analysis and related reference [22], the $E_{Pb(II)/Pb}$ in ChCl–urea DES can be presented by Eq. (2). Since the Pb(II) concentration on electrode surface C' Pb(II)

and in bulk solution $C_{Pb(II)}$ are basically same at the incipient stage of the reduction process, this two parameters are assumed as equal in values.

$$
\begin{aligned}
E_{Pb(II)/Pb} &= E^0_{Pb(II)/Pb} + \frac{RT}{2F} \ln \left(\gamma_{Pb(II)} \times C'_{Pb(II)} \right) \\
&= E^0_{Pb(II)/Pb} + \frac{RT}{2F} \ln \left(\gamma_{Pb(II)} \times C_{Pb(II)} \right)
\end{aligned}
\tag{2}
$$

where the unit of $C_{Pb(II)}$ and C' Pb(II) is mol cm^{-3}; $E_{Pb(II)/Pb}$ is the reduction potential of Pb(II)/Pb, V; $E0$ Pb(II)/Pb is the standard electrode potential of Pb(II)/Pb, V; $\gamma_{Pb(II)}$ is the activity coefficient of Pb(II); F is the Faraday constant; R is the gas constant and T is the absolute temperature, K. From Eq. (2), the $E_{Pb(II)/Pb}$ has good linear with the logarithm of Pb(II) concentration $\ln C_{Pb(II)}$, when the activity coefficient is a constant. The relationship between $E_{Pb(II)/Pb}$ and $\ln C_{PbS}$ is shown in Fig. 2d, which demonstrates that higher PbS concentration contributes to the reduction of Pb(II). The different slopes between that of MS and GC electrode also indicate that the effect of PbS concentration on the reduction of lead is more significant on GC electrode. Therefore, the lead powders with different dimensions and morphologies can be obtained through controlling the PbS concentration of PbS–ChCl–urea solution. As described in the literature [25], the current density during the deposition process can strongly affect the final shape of deposits and the forms of electrodeposited metallic powders are usually dendritic, flakes, needles, spongy or fibers, etc.

3.2 Chronoamperometric analysis

The nucleation and growth process of lead powders have been investigated by chronoamperometry measurement on MS electrode in 50 mM PbS–ChCl–urea DES at 353 K, as illustrated in Fig. 3a. According to Scharifker [26], the current increases rapidly to a maximum value in a short time, resulting from the increasing of electroactive area with the raising of nuclei numbers. At this stage, hemispherical mass transfer of metal ions is formed. After that, a slow decay of current transients is observed in a long period, resulting from the overlapped diffusion zones around nuclei. When the substrate surface can be covered completely with diffusion zones, the diffusion layer

should be uniform and the curves should follow the Cottrell equation. All curves can be analyzed according to the three-dimensional (3D) nucleation model for diffusion-controlled process, which is classified into instantaneous and progressive nucleation process [26]. The dimensionless forms for the instantaneous and progressive 3D nucleation are given in Eqs. (3) and (4) respectively, where i_m is the peak current density and t_m is the corresponding time at i_m. Figure 3b shows the relationship between the $(i/i_m)^2$ and the t/t_m at different potentials. In comparison with the theoretical transients, the simulated curves are similar with the model of instantaneous nucleation process. It is suggested that the electrocrystallization of lead on MS electrode at each applied potential through formation of active sites can be considered as an instantaneous nucleation process under diffusion control. The instantaneous nucleation refers to that all nucleation sites are activated at the same moment after the potential stepped to a sufficient value. And this will lead to the formation of fine lead grains. It is agreement with the results reported by Katayama et al. [16] in BMPTFSA ionic liquid containing Pb(TFSA)$_2$ and Reddy et al. [27] in PbO–urea-BMIC. Then, the diffusion coefficient for the instantaneous nucleation process can be calculated by Eq. (5) [28] and the experimental values of i_m and t_m from Fig. 3. The diffusion coefficient is about 2.40×10^{-7} cm^2/s and in good agreement with the data reported by Reddy et al. [28] (6.56×10^{-7} cm^2/s).

$$\left(i/i_m\right)^2 = 1.9542\left\{1 - \exp\left[-1.2564\left(t/t_m\right)\right]\right\}^2\left(t/t_m\right)^{-1} \tag{3}$$

$$\left(i/i_m\right)^2 = 1.2254\left\{1 - \exp\left[-2.3367\left(t/t_m\right)\right]\right\}^2\left(t/t_m\right)^{-1} \tag{4}$$

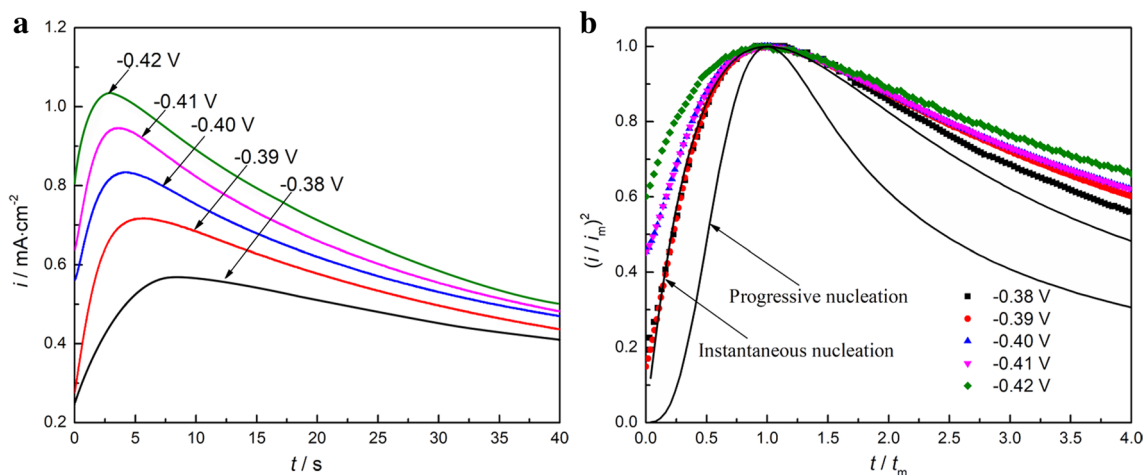$$i_m^2 t_m = 0.1629(nFC)^2 D \tag{5}$$

Fig. 3 **a** Current transient curves of MS electrode in 50 mM PbS–ChCl–urea DES at 353 K, **b** dimensionless plot of $(i/i_m)^2$ versus t/t_m using the data of **a**, with theoretical models for diffusion-controlled 3D instantaneous and progressive nucleation

3.3 Morphology analysis

In general, the morphology of deposits largely depends on the experimental parameters and the inherent characteristics of metals. Figures 4 and 5 are the SEM and TEM micrographs of electrodeposited lead powders on MS substrate at 2.5 V and 353 K for 2 h with PbS concentrations from 10 to 50 mM. From Fig. 4a, three-dimensional sub-micrometer lead particles are agglomerated together at 10 mM PbS concentration. This can be attributed to the differences of the overpotential distribution and the local PbS concentration on the nuclei and grains surface [10]. From the magnification of Fig. 4b, these coral-like powders are composed of many overlapped sub-micrometer lead particles about 150–200 nm. TEM micrographs (Fig. 4c) show that these particles are flake-like and densely agglomerate with each other. A well-defined plane formed by ordered stacking

with a d spacing of 0.28 nm, as illustrated in Fig. 4d. The selected area diffraction pattern shows the diffraction spots indexed as (111) plane without any trace of a secondary phase. At 20 mM, the morphology of lead powders are basically the same as before, but the particle size of the flake-like sub-micrometer particles is significantly enlarged to 400–550 nm (Fig. 4e, f). With the increasing of PbS concentration from 30 to 50 mM (Fig. 5), the coral-like lead powders are increased slightly in particle size and their pores are gradually occupied by lots of sub-micrometer lead flakes. As clearly can be seen from the magnification of Fig. 5d, the surface of these lead particles are covered and encapsulated by many fine grains in 50–120 nm, so that the surface of these particles is smoother than that obtained at lower PbS concentration (Fig. 4a).

According to above discussion, the PbS concentration has obvious effect on the deposited lead powders in both
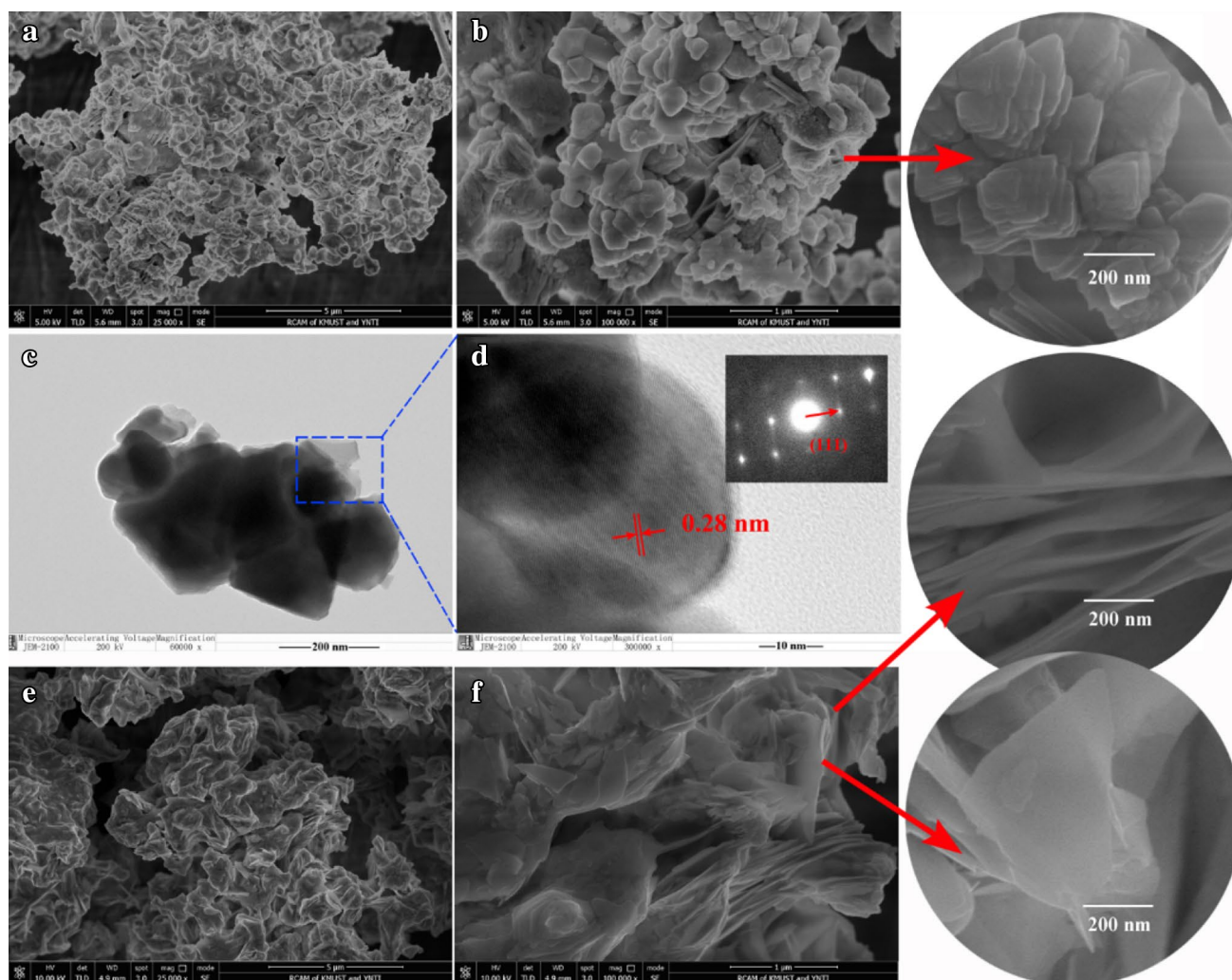

Fig. 4 SEM and TEM micrographs of lead powders electrodeposited at 2.5 V and 353 K for 2 h with different PbS concentrations: **a–d** 10 mM, **e, f** 20 mM
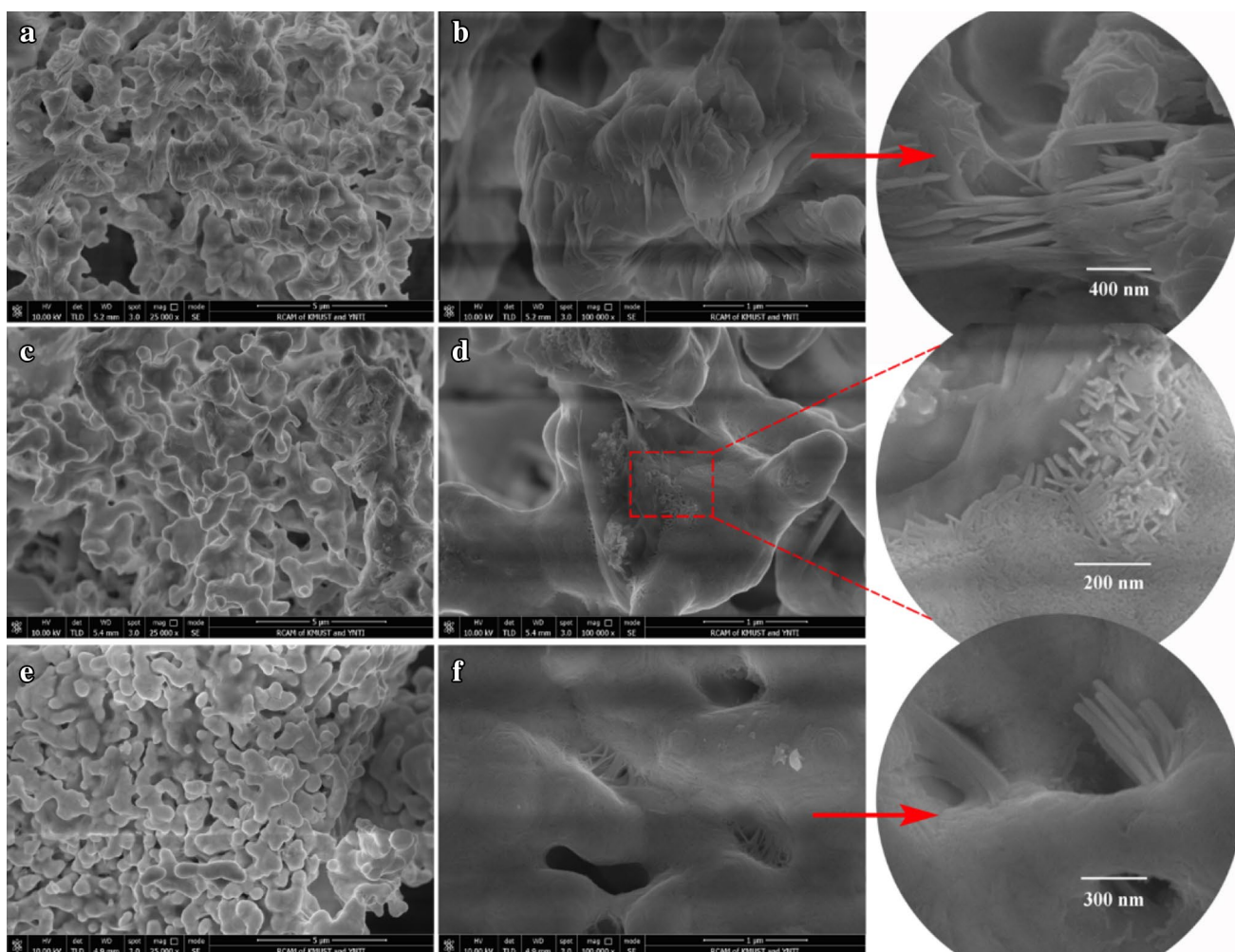
Fig. 5 SEM micrographs of lead powders electrodeposited at 2.5 V and 353 K for 2 h with different PbS concentrations: **a, b** 30 mM, **c, d** 40 mM, **e, f** 50 mM

particle size and morphology. At lower PbS concentration, finer lead powders are deposited due to the lower ion concentration on the electrode surface. The new nuclei are more easily absorbed onto the edges and corners where the surface energy is higher, so that it can be reduced to minimum. Thus, these newly formed crystals are inclined to distribute on the surface of the lead particles. With increasing PbS concentration, the $E_{Pb(II)/Pb}$ become positive than before (Fig. 2), resulting in the raising of current density and reduction rate under the same applied cell voltage. The newly crystallization center with some dislocations and twinning crystal defects will generate on the lead particles. Thus, sub-micrometer lead flakes and fine lead grains are formed on the surface and pores of larger lead particles. Consequently, coral-like lead powders in different particle sizes and porosity can be deposited through controlling PbS concentration in the solution.

3.4 Composition and crystal structure of lead powders

The crystal structure and phase composition of the lead powders, which are electrodeposited from PbS–ChCl–urea solution at 2.5 V cell voltage and 353 K with different PbS concentrations (10–50 mM), are analyzed by XRD, as presented in Fig. 6a. The deposited lead powders are consistent with a face-centered-cubic structure and JCPDS standard card (004-0686). The strongest peak intensity of the lead crystallites is (111) plane, which is consistent with the TEM result (Fig. 4d). Apart from this, the (200), (220), (311), (222), (331), and (420) planes are also presented. The particle size of the lead powders could be calculated using Scherrer's formula [29].

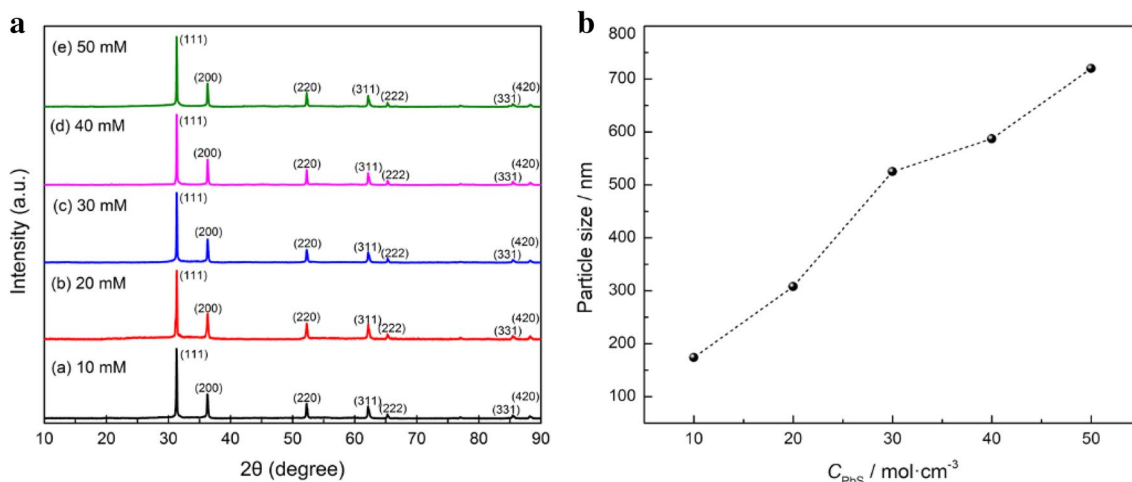$$D = \frac{K\lambda}{B \cos \theta} \tag{6}$$

Fig. 6 **a** XRD of lead powders electrodeposited at 2.5 V and 353 K for 2 h with different PbS concentrations, as indicated; **b** effect of C_{PbS} on the particle size of Pb powders

where D is the average size of particles; $K = 1.0$; λ is the wavelength of X-ray radiation, $\lambda = 0.154056$ nm; B is the full width at half maximum of the diffracted peak; and θ is the angle of diffraction. The sizes of the lead powders as a function of C_{PbS} are shown in Fig. 6b. When the PbS concentrations is 10 mM in PbS–ChCl–urea solution, the average particle size of lead powders is around 174.1 nm. When the PbS concentration is increased from 20 to 30 mM, the particle size is increased significantly from 308.4 nm to 525.2 nm. With the increasing of PbS concentration to 50 mM, the size of lead powders is increased to 720.3 nm. It is found that the higher PbS concentration can promote the growth of particles which is consistent with the conclusions above mentioned.

4 Conclusions

(1) Sub-micrometer lead powders have been electrodeposited on mild steel substrate in PbS-containing (10–50 mM) ChCl–urea DES at 353 K and 2.5 V for 2 h.

(2) Cyclic voltammetry on MS and GC electrodes demonstrate that the increase in PbS concentration can effectively facilitate the shift of the reduction potential $E_{Pb(II)/Pb}$ in positive direction. By comparison, the reduction of Pb(II) on GC electrode is more difficult than that on MS electrode, so the electrodeposition of lead powders on active electrode will benefit to the nucleation of lead grains.

(3) The electrocrystallization of metallic lead at the early stage can be explained through a three-dimensional instantaneous nucleation under diffusion control. And the diffusion coefficient of Pb(II) at 353 K is about 2.40×10^{-7} cm^2/s.

(4) The morphology of deposited lead is coral-like and porous structure which mainly composed of many overlapped sub-micrometer lead flakes about 150–200 nm. With elevated PbS concentration, the particle size of lead powders is increased slightly and their surface and pores are gradually occupied by lots of lead sub-micrometer particles.

(5) The crystallites of lead powders are predominately oriented in (111) plane, and the particle size has been calculated using Scherrer's formula. Higher PbS concentration can promote the growth of particles, which is increased significantly from 174.1 to 720.3 nm.

References

1. Popov KI, Stojilković ER, Radmilović V, Pavlović MG (1997) Morphology of lead dendrites electrodeposited by square-wave pulsating overpotential. Powder Technol 93:55–61

2. Ji K, Chen X, Zhao H, Dai Z (2014) Electrodeposited lead-foam grids on copper-foam substrates as positive current collectors for lead-acid batteries. J Power Sources 248:307–316

3. Riminucci A, Schwarzacher W (2014) Magnetic signature of granular superconductivity in electrodeposited Pb nanowires. J Appl Phys 115:777–787

4. Orhan G, Hapçı G (2010) Effect of electrolysis parameters on the morphologies of copper powder obtained in a rotating cylinder electrode cell. Powder Technol 201:57–63

5. German RM (1994) Powder metallurgy science. Metal Powder Industries Federation, Princeton

6. Lou W, Cai W, Li P, Su J, Zheng S, Zhang Y, Jin W (2018) Additives-assisted electrodeposition of fine spherical copper powder from sulfuric acid solution. Powder Technol 326:84–88

7. Nikolić ND, Ivanović ER, Branković G, Lačnjevac U, Stevanović SI, Stevanović JS, Pavlović MG (2015) Electrochemical and crystallographic aspects of lead granular growth. Metall Mater Trans B 46:1760–1774

8. Nikolić ND, Popov KI, Živković PM, Branković G (2013) A new insight into the mechanism of lead electrodeposition: ohmic-diffusion control of the electrodeposition process. J Electroanal Chem 691:66–76

9. Wang J, Wang H, Han Z, Han J (2015) Electrodeposited porous Pb electrode with improved electrocatalytic performance for the electroreduction of CO_2 to formic acid. Front Chem Sci Eng 9:57–63

10. Cherevko S, Xing X, Chung CH (2011) Hydrogen template assisted electrodeposition of sub-micrometer wires composing honeycomb-like porous Pb films. Appl Surf Sci 257:8054–8061

11. Nikolić ND, Branković G, Lačnjevac U (2011) Formation of two-dimensional (2D) lead dendrites by application of different regimes of electrolysis. J Solid State Electrochem 16:2121–2126

12. Wranglén G (1960) Dendrites and growth layers in the electrocrystallization of metals. Electrochim Acta 2:130–143

13. Smith EL, Abbott AP, Ryder KS (2014) Deep eutectic solvents (DESs) and their applications. Chem Rev 114:11060–11082

14. Abbott AP, Capper G, Davies DL, Rasheed RK, Tambyrajah V (2003) Novel solvent properties of choline chloride/urea mixtures. Chem Commun 9:70–71

15. Pershin P, Yu K, Arkhipov P, Yu Z (2014) The electrodeposition of lead in $LiCl$-KCl-$PbCl_2$ and $LiCl$-KCl-$PbCl_2$-PbO melts. J Electrochem Soc 161:D824–D830

16. Katayama Y, Fukui R, Miura T (2013) Electrodeposition of lead from 1-butyl-1-methylpyrrolidinium Bis(trifluoromethylsulfonyl) amide ionic liquid. J Electrochem Soc 160:D251–D255

17. Ru J, Hua Y, Wang D (2017) Direct electro-deoxidation of solid PbO to porous lead in choline chloride-ethylene glycol deep eutectic solvent. J Electrochem Soc 164:D143–D149

18. Ru J, Hua Y, Wang D, Xu C, Zhang Q, Li J, Li Y (2016) Dissolution-electrodeposition pathway and bulk porosity on the impact of in situ reduction of solid PbO in deep eutectic solvent. Electrochim Acta 196:56–66

19. He W, Liu A, Guan J, Shi Z, Gao B, Hu X, Wang Z (2017) Pb electrodeposition from PbO in the urea/1-ethyl-3-methylimidazolium chloride at room temperature. RSC Adv 7:6902–6910

20. Yang H, Reddy RG (2015) Electrochemical kinetics of reduction of zinc oxide to zinc using 2:1 urea/ChCl ionic liquid. Electrochim Acta 178:617–623

21. Xie X, Zou X, Lu X, Zheng K, Cheng H, Xu Q, Zhou Z (2016) Voltammetric study and electrodeposition of Cu from CuO in deep eutectic solvents. J Electrochem Soc 163:D537–D543

22. Tachikawa N, Serizawa N, Katayama Y, Miura T (2008) Electrochemistry of Sn(II)/Sn in a hydrophobic room-temperature ionic liquid. Electrochim Acta 53:6530–6534

23. Tsuda T, Boyd LE, Kuwabata S, Hussey CL (2010) Electrochemistry of copper(I) oxide in the 66.7–33.3 mol % urea-choline chloride room-temperature eutectic melt. J Electrochem Soc 157:F96–F103

24. Bard AJ, Faulkner LR (2001) Electrochemical methods: fundamentals and applications, 2nd edn. Wiley, New York

25. Nikolic N, Maksimovic V, Brankovic G, Zivkovic P, Pavlovic M (2013) Influence of the type of electrolyte on the morphological and crystallographic characteristics of lead powder particles. J Serb Chem Soc 78:1387–1395

26. Scharifker B, Hills G (1983) Theoretical and experimental studies of multiple nucleation. Electrochim Acta 28:879–889

27. Liu A, Shi Z, Reddy RG (2017) Electrodeposition of Pb from PbO in urea and 1-butyl-3-methylimidazolium chloride deep eutectic solutions. Electrochim Acta 251:176–186

28. Yang H, Reddy RG (2014) Electrochemical deposition of zinc from zinc oxide in 2:1 urea/choline chloride ionic liquid. Electrochim Acta 147:513–519

29. Arrhenius G (1954) X-ray diffraction procedures for polycrystalline and amorphous materials. Wiley, New York

Affiliations

Juanjian Ru[1] · Jiaojiao Bu[1] · Zhiwei Wang[1] · Yixin Hua[1,2] · Ding Wang[1]

✉ Ding Wang
   wangdingliverpool@foxmail.com

[1] Faculty of Metallurgical and Energy Engineering, Kunming University of Science and Technology, Kunming 650093, China

[2] State Key Laboratory of Complex Nonferrous Metal Resources Clean Utilization, Kunming 650093, China